Direct potential and temperature effects on the MgHe line-core and far-wing photoabsorption profiles

L. Reggami[1] and M. Bouledroua[2]
[1]*Physics Department, Badji Mokhtar University, B.P. 12, Annaba 23000, Algeria*
[2]*Laboratoire de Physique des Rayonnements, Badji Mokhtar University, B.P. 12, Annaba 23000, Algeria*
(Received 29 August 2010; published 30 March 2011)

The present study deals with the collisional broadening of monatomic magnesium, evolving in a helium buffer gas, in the wavelength and temperature ranges 260–310 nm and 100–3000 K, respectively. The computed emission and absorption spectral profiles are based on the most recent potential-energy curves and transition dipole moments. The required interatomic $Mg(3s^2) + He(1s^2)$ and $Mg(3s3p) + He(1s^2)$ potentials are constructed from two different sets. The purpose of this treatment is twofold. First, using the quantum-mechanical Baranger impact approximation, the width and shift of the line-core spectra are determined and their variation law with temperature is examined. Then, the satellite structures in the blue and red wings are analyzed quantum mechanically. The calculations show especially that the free-free transitions contribute most to the MgHe photoabsorption spectra and that a satellite structure is observable beyond the temperature 1800 K around the wavelengths 272 or 276 nm, depending on the used potential set. Weak satellites have also been investigated and, for all cases, the obtained results showed good agreement with those already published.

DOI: 10.1103/PhysRevA.83.032719 PACS number(s): 34.20.Cf, 32.30.Jc, 33.70.Jg, 51.20.+d

I. INTRODUCTION

The investigation of pressure broadening phenomena is a recognized method commonly employed in molecular spectroscopy to generate, identify, and assess interatomic potentials. The spectroscopic analysis and measurements realized up to now have, indeed, proved the sensitivity of the spectral parameters to the potentials and transition dipole moments (TDMs) and established the existence of strong correlations with their microscopic details [1,2]. Moreover, the absorption spectral investigations of atoms, including the alkali metals [3,4] and the alkaline-earth metals [5,6], embedded in large helium clusters are, in the last few years, among the other methods usually used for probing the diatomic potentials [7–9]. It is indeed demonstrated that the microstructure and physical features of the atom-doped helium clusters rely basically on pairwise additive models, in which the atom-atom potential-energy curves are utilized [10]. Alternatively, much attention has been devoted in recent decades to the collisional shifts and broadening of the resonance line of alkali-metal atoms perturbed by parent [11–17] or foreign [18–25] gases. But fewer efforts have been undertaken to study theoretically or experimentally the line broadening of two-electron alkaline-earth-metal atoms in buffer gases [26–29].

This work proposes to make use of two different potential sets to treat theoretically the collisional broadening of the alkaline-earth magnesium $3s^2 - 3s3p$ transition line perturbed by ground helium and examine their effects on the *line core* and the *far wings* of the emission and absorption spectra. *Full,* but *simplified,* quantum-mechanical calculations are more specifically performed to look at the role the potentials and temperature can have in the determination of the spectral profile, shape, and position, and at the possible occurrence of satellite structures in the wings.

We describe in this paper the construction of the potentials involved in the interactions $Mg(3s3p \leftarrow 3s^2) + He(1s^2)$ from the most recent and reliable theoretical ground and excited potential data points. The lack of Rydberg-Klein-Rees potentials, which are based on spectroscopic observations, requires from us to rather use for such systems *ab initio* data, which thus constitutes, as stated in [30], a valuable test of the theoretical methods and their outputs. Besides, since the ground $3s^2\ ^1S_0$ and the first excited $3s3p\ ^1P_1$ states of magnesium are connected with corresponding electric transition dipole moments, a part of this work is devoted to their construction in the long- and short-range distances. The quality of the potentials as well as of the transition dipole moments and the obtained numerical wave functions is verified by checking the values of the rotational-vibrational states, the lifetime of the excited level, and the temperature-dependant collision integrals and diffusion coefficients. Once all the above is done, the line-core broadening and shifting and the far-wing spectra of the magnesium monatoms perturbed by helium are extensively studied. The results are reported and analyzed in order to interpret the potential and temperature effects and to identify the spectral satellite positions and intensities. Unless otherwise stated, atomic units (a.u.) are used throughout this paper.

II. THEORY

It is well known from atomic and molecular spectroscopy [1,2] that, when an absorbing or emitting atom is undergoing interactions with the atoms of its surrounding environment, the spectral profile experiences generally two important phenomena: (i) the broadening, generally accompanied with shifting, of the line-core spectra, and (ii) the appearance of a satellite structure in the red and/or blue wings. These two phenomena are well described theoretically and their quantal results are summed up here below.

In this work, we are more precisely interested in the pressure broadening which a magnesium ^{24}Mg undergoes while interacting with a ground helium $He(1s^2)$. We shall in particular consider the effects on the line core of the spectra

when an excited Mg($3s3p\ ^1P_1$) emits a photon and on their far wings when a ground Mg($3s^2\ ^1S_0$) absorbs a photon.

A. Line-core broadening

In setting up his *simplified* quantum-mechanical theory of pressure broadening, Baranger [31] made several important assumptions, including (i) both atomic states involved in emission are nondegenerate, (ii) the collisions between the emitting atoms and the perturbers are elastic, and (iii) the buffer gas mainly consisting of the perturbers is dilute, that is, the collisions are typically binary and their duration is much smaller than the duration between two successive collisions. This latter presupposition constitutes the so-called impact approximation under which the radiated line has a Lorentzian shape.

So, within the frames of the simplified quantum-mechanical impact approximation, the full width at half maximum w and the shift of the line core d are given in terms of the cross sections $\sigma_w(E)$ and $\sigma_d(E)$ effective, respectively, in width and shift as [31]

$$w = +n\langle v\sigma_w\rangle_{\rm av}, \tag{1}$$

$$d = -n\langle v\sigma_d\rangle_{\rm av}, \tag{2}$$

where n is the number density, assumed very low, of the perturbing gas and v is the relative velocity related to the energy $E = \frac{1}{2}\mu v^2$, with μ being the reduced mass of the interacting atomic pair. In both equations, the brackets $\langle\cdots\rangle_{\rm av}$ denote the average value calculated over the thermal Maxwellian distribution. The width and shift cross sections are defined by the sums [2,31]

$$\sigma_w = \frac{4\pi}{k^2}\sum_{l=0}^{\infty}(2l+1)\sin^2(\eta_l' - \eta_l''), \tag{3}$$

$$\sigma_d = \frac{\pi}{k^2}\sum_{l=0}^{\infty}(2l+1)\sin[2(\eta_l' - \eta_l'')], \tag{4}$$

where $k = \sqrt{2\mu E}/\hbar$ is the magnitude of the wave-number vector $\mathbf{k}$ and l is the angular momentum. The lower $\eta_l''(E)$ and upper $\eta_l'(E)$ phase shifts, both required for the computation of the cross sections σ_w and σ_d, are determined by solving the radial wave equation

$$\frac{d^2}{dR^2}\Phi_l(R) + \left[k^2 - \frac{2\mu}{\hbar^2}V(R) - \frac{l(l+1)}{R^2}\right]\Phi_l(R) = 0, \tag{5}$$

in which the radial wave functions $\Phi_l(R)$ are forced to be identified with the asymptotic form

$$\Phi_l(R) \sim \sin\left(kR - \frac{l}{2}\pi + \eta_l\right). \tag{6}$$

In Eqs. (5) and (6), $\hbar$ is the reduced Planck's constant and $V(R)$ is the potential energy at the interatomic separation R. It is noteworthy to mention here that more complete models which deal accurately with pressure broadening and shifting are available and have been essentially applied to special systems [32–34].

B. Far-wing broadening

During any photoabsorption process, the absorber-perturber system witnesses in general four possible transitions, namely, *bound-bound, bound-free, free-bound,* and *free-free,* from a lower electronic state, noted hereafter with a double prime, to an upper electronic state, noted with a single prime. According to the Beer-Lambert law, this process may be characterized via the photoabsorption coefficient $k(\nu)$, with ν being the frequency of the absorbed photon.

For the specific case of the MgHe system, the main contribution to the global absorption coefficient comes almost exclusively from the free-free transitions. This is mainly because the ground and excited potential-energy curves, as it will be seen in the next section, are very shallow. If we denote by $n_{\rm Mg}$ and $n_{\rm He}$ the number densities of the absorber Mg and perturber He in the gas mixture at temperature T, one may define the *reduced* photoabsorption coefficient as $k_r(\nu) = k(\nu)/n_{\rm Mg}n_{\rm He}$. Furthermore, let ν_0 denote the *unperturbed* frequency of the Mg($3s3p \leftarrow 3s^2$) line. So, during the absorption of a photon of energy $h\nu = \epsilon' - \epsilon'' + h\nu_0$, the absorber-perturber quasimolecule undergoes a transition from the lower electronic state (ϵ'', J'') to the upper electronic state (ϵ', J'), both connected by the transition dipole moment $D(R)$. In such a case, the reduced free-free photoabsorption coefficient is given by [12,35]

$$k_r(\nu) = \frac{8\pi^3\nu}{3c}\varpi\left(\frac{2\pi\hbar^2}{\mu k_B T}\right)^{3/2}\sum_J(2J+1) \times \int_0^{\infty}|\langle\Phi_{\epsilon',J}|D(R)|\Phi_{\epsilon'',J}\rangle|^2\exp(-\epsilon''/k_BT)\,d\epsilon', \tag{7}$$

where J is the total angular momentum assumed here to be very high, thus $J = J' \simeq J''$, and ϵ is the positive energy of the corresponding free state (ϵ, J), associated with the *energy*-normalized wave functions $\Phi_{\epsilon,J}(R)$. Strictly speaking, the total electronic orbital angular momentum $\mathbf{L}$ and the electron spin $\mathbf{S}$ are coupled but very weakly and the it can be ignored [33,36]. Grycuk *et al.* [37] and Behmenburg *et al.* [38] came to this conclusion when they stated that, over the temperature range of interest, the spin-orbit coupling is very weak and the electron spin contribution to the total angular momentum J is neglected. Accordingly, J is equivalent to a quantum number N in Hund's case (b) [39]. The wave functions $\Phi_{\epsilon,J}(R)$ can be determined by solving the radial wave equation for the relative motion of the nuclei

$$\frac{d^2}{dR^2}\Phi_{\epsilon,J}(R) + \frac{2\mu}{\hbar^2}\left[\epsilon - V(R) - \frac{\hbar^2}{2\mu}\frac{J(J+1)-\Lambda^2}{R^2}\right]\Phi_{\epsilon,J}(R) = 0, \tag{8}$$

with Λ being the component of $\mathbf{L}$ over the internuclear axis. Numerically, $\Lambda = 0$ for the Σ states and $\Lambda = 1$ for the Π states. In Eq. (7) above, c and k_B have their usual meaning and ϖ is the probability the absorber-perturber system possesses in forming a molecule in the lower electronic state.

TABLE I. Potential short- and long-range parameters in a.u. All the dispersion coefficients, C_n, are from Mitroy and Zhang [44].

	A		B		Dispersion coefficients		
Molecular state	Set I	Set II	Set I	Set II	C_6	C_8	C_{10}
$X\,^1\Sigma^+$	4.32	3.87	1.28	1.38	21.45	884.00	3.933×10^4
$A\,^1\Pi$	0.87	28.2	1.24	2.37	43.41	995.30	4.200×10^4
$B\,^1\Sigma^+$	0.30	3.53	0.61	1.45	77.75	10 520	1.445×10^6

III. MAGNESIUM-HELIUM SYSTEM

To perform the needed investigations, the MgHe potential-energy curves $V(R)$ and the transition dipole moments $D(R)$ are both required. The ground $Mg(3s^2)$ approaches $He(1s^2)$ along the unique singlet potential-energy curve $X\,^1\Sigma^+$. The photoabsorption scheme

$$Mg(3s^2) + He(1s^2) + h\nu \longrightarrow Mg(3s3p) + He(1s^2)$$

leads the excited $Mg(3s3p)$ to interact with the ground helium along two possible singlet potential-energy curves, $A\,^1\Pi$ and $B\,^1\Sigma^+$, dismissing the triplet molecular states forbidden by the quantal selection rules [39].

A. Potential-energy curves

We used, to construct each of the X, A, and B potential-energy curves, two sets of newly computed data points, designated hereafter as set I and set II.

1. Set I potentials

The MgHe potential-energy curves are based on the very recent data points borrowed from Hinde [40] for the ground state and from Mella *et al.* [41] and Reho *et al.* [42] for the excited states. For the ground curve, we used the Hinde data [40] for the distances $5.67 \lesssim R \lesssim 22.68$. The construction produced a value of $D_e = 4.73\,\mathrm{cm}^{-1}$ for the dissociation energy at the equilibrium separation $R_e = 9.7$. For the excited states, we have constructed the $A\,^1\Pi$ symmetry upon the data points ranging from $R = 5.67$ to $R = 19.84$ from Mella *et al.* [41] which we extrapolated, in the short range, with those of Reho *et al.* [42] for $3.8 \leqslant R \leqslant 5.3$. A dissociation energy $D_e = 39.64\,\mathrm{cm}^{-1}$ and an equilibrium distance $R_e = 7.2$ are found for this case. The $B\,^1\Sigma^+$ state has been constructed solely from the data of Mella *et al.* [41] in the range $5.67 \leqslant R \leqslant 17.95$. The construction yields the values $D_e = 0.77\,\mathrm{cm}^{-1}$ and $R_e = 16.3$.

2. Set II potentials

All the potentials here have been entirely constructed from the data points published in Paul-Kwiek and Czuchaj [27] and provided to us by Paul-Kwiek. Adopting their potential values for the internuclear distances ranging from 2.75 to 14, the $X\,^1\Sigma^+$ curve could produce a well with the depth $D_e = 3.85\,\mathrm{cm}^{-1}$ located at the position $R_e = 10.5$. For both $A\,^1\Pi$ and $B\,^1\Sigma^+$ states, the constructions used the data points in the range $2.75 \leqslant R \leqslant 18$ which yielded the well depths 19.50 and $1.28\,\mathrm{cm}^{-1}$ corresponding to the equilibrium positions 8.1 and 16.5, respectively.

Finally, it is important to notice that the larger values of D_e for the $^1\Pi$ versus $^1\Sigma^+$ states, found with both set I and set II potentials, are likely attributed to the existence of a nodal plane that contains the magnesium nucleus, thus permitting closer approach of the closed-shell helium atom.

3. Potential constructions

In all cases, the potentials have been constructed by slightly modifying and appropriately connecting all the data points to match with the relationship

$$V(R) = -\frac{C_6}{R^6} - \frac{C_8}{R^8} - \frac{C_{10}}{R^{10}}, \tag{9}$$

in the long-range region, and with the Born-Mayer form

$$V(R) \sim A\exp(-BR), \tag{10}$$

in the short-range region [43]. The constants C_6, C_8, and C_{10} are the dispersion coefficients and A and B are two constant parameters. The dispersion coefficients, adopted from the recent calculations of Mitroy and Zhang [44], and our computed values of A and B are reported for the X, A, and B states in Table I.

The constructed MgHe, sets I and II, potential-energy curves are shown in the upper line of Fig. 1, through which one may notice they are all very shallow. We also present in the lower line of the same figure the potential differences $\Delta V_{A-X}(R)$ and $\Delta V_{B-X}(R)$. These differences, transformed in terms of the wavelength λ, exhibit some extrema which *classically* mean the possible appearance in the *blue* wing of a satellite near 273 nm when the set I potentials are used and near 268 nm with the set II potentials. Whereas, in the *red* wing, the calculations foresee the exhibition of a satellite structure around 413 nm when set II is used, but nothing is expected with set I. At such extremum positions, the perturber He applies the same force on the atomic absorber Mg, whether the latter is in its ground or excited state, and the classical expression for the photoabsorption coefficient becomes singular [2].

B. Transition dipole moments

The construction of the transition dipole moments $D(R)$ follows in general the same steps as the ones used for the potential-energy curves. For this sake, we selected exclusively the values of Paul-Kwiek and Czuchaj [27] over the intervals $3.0 \leqslant R \leqslant 12.0$, for the $X\,^1\Sigma^+ \rightarrow A\,^1\Pi$ transition, and $3.0 \leqslant R \leqslant 20.0$, for the $X\,^1\Sigma^+ \rightarrow B\,^1\Sigma^+$ transition. All these data are smoothly and suitably connected in the long-range regions to the analytical form $D(R) \sim D_\infty + \gamma/R^6$, where D_∞ is the asymptotic value of $D(R)$, chosen here as $D_\infty = 2.343$ [27]. For the short internuclear distances, we forced the transition

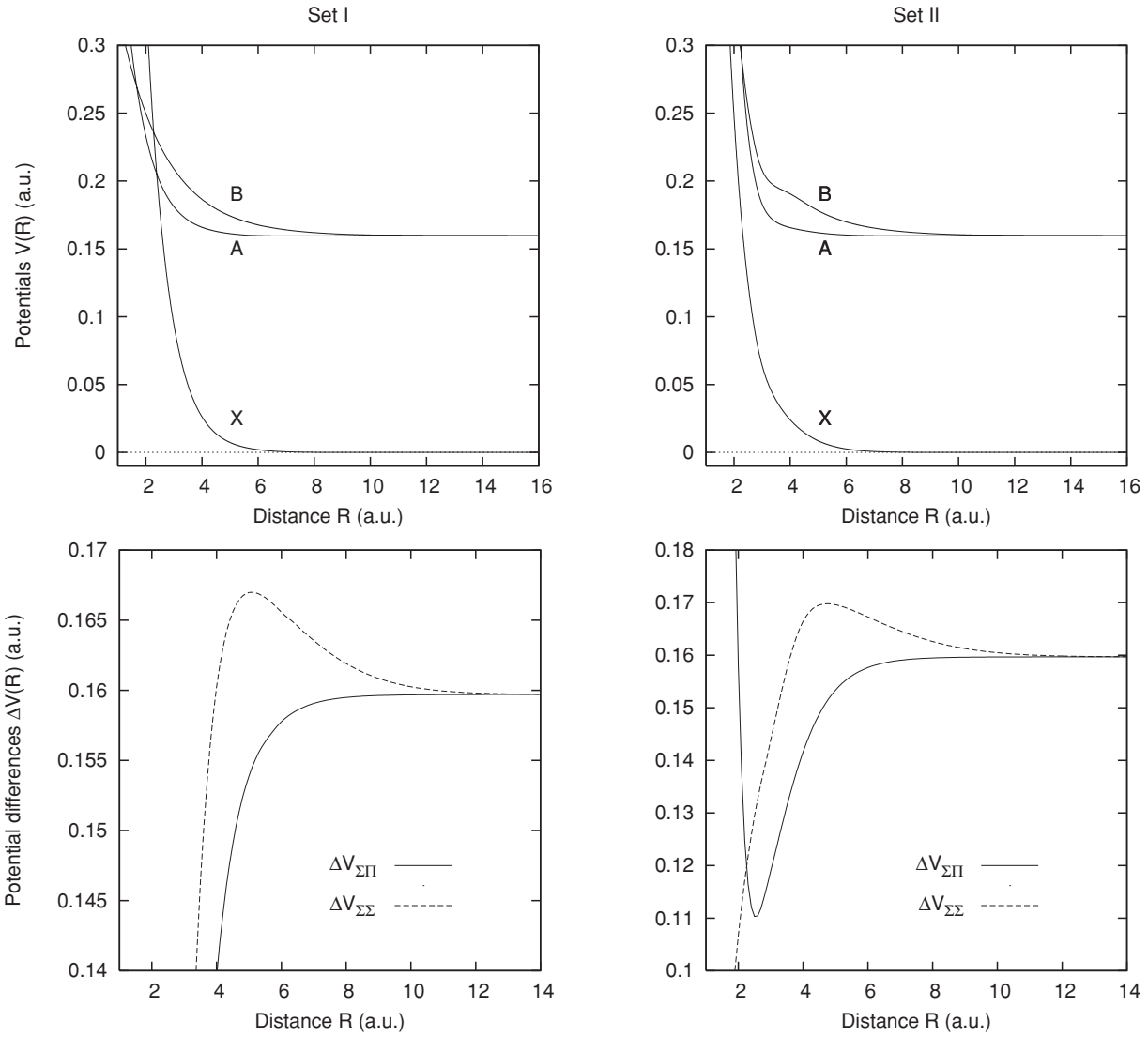

FIG. 1. Potential-energy curves and difference potentials relative to the ground, $X\ ^1\Sigma^+$, and the two first excited, $A\ ^1\Pi$ and $B\ ^1\Sigma^+$, states of the MgHe system. The upper graphs represent the set I and II potential-energy curves. The lower graphs are the plots representing the potential differences $\Delta V_{\Sigma\Pi} = \Delta V_{A-X}(R)$ and $\Delta V_{\Sigma\Sigma} = \Delta V_{B-X}(R)$.

dipole moments to behave linearly like $D(R) \sim a + bR$. The adopted values of γ, a, and b are listed in Table II and the curves of the constructed transition dipole moments are displayed in Fig. 2, from which one can remark that both moments get almost the same value D_∞ beyond $R \simeq 8$.

IV. POTENTIAL AND TDM ASSESSMENTS

To authenticate the quality of our constructed potentials, we propose to compute with these potentials some physical parameters, such as the rovibrational states and the radiative lifetime of the atomic excited level, and to analyze the temperature-dependant thermophysical properties, namely, the collision integrals and the diffusion coefficients.

TABLE II. Constant parameters adopted for the constructed transition dipole moments $D(R)$ in both long- and short-range regions.

Transition	γ	a	b
$\Sigma\Sigma$	$+1.31 \times 10^4$	$+1.697$	-0.123
$\Sigma\Pi$	-613.473	$+2.065$	$+0.047$

A. Rovibrational states

One of the best methods used to assess the quality of the constructed potentials is to determine their rotational-vibrational states and examine how they compare with the published values. For this purpose, we adapted with some alterations the subcode Automatic Level Finder (ALF) implemented in the well-known Le Roy's package LEVEL 7.4 [45]. Our computed values for the two ground and excited MgHe states are listed in Table III.

Although the potential curves seem to be very shallow and practically repulsive, the calculations revealed the existence of a very limited number of rotationless vibrational levels. Indeed, for the X curve, whether constructed upon the set I or set II data, we could detect just one single level. This is also the

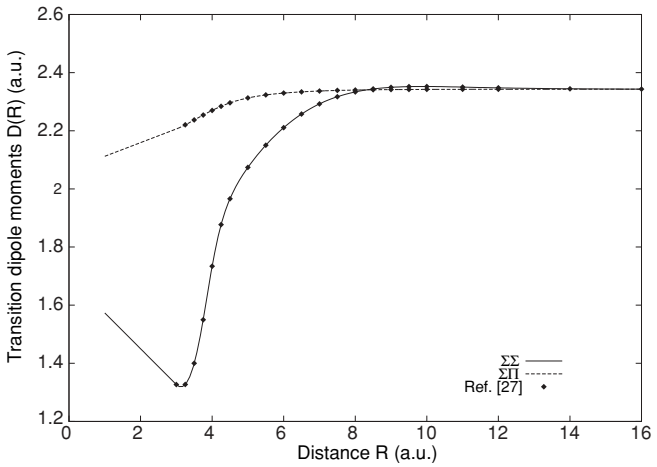

FIG. 2. Electronic transition dipole moments that connect the MgHe ground state $X\ ^1\Sigma^+$ to the excited states $A\ ^1\Pi$ and $B\ ^1\Sigma^+$. The data points upon which these TDMs are constructed are from Ref. [27].

case with the A curve, where we found three levels when set I was employed and two levels when set II was employed. The same number of the rotationless vibrational levels could also be found by application of the semiclassical method developed by Gribakin and Flambaum [46]. For the B state, no levels were found. Table III displays also the energy in cm^{-1} of the rovibrational levels, which we compare, for the ground state, with those published in Lovallo and Klobukowski [30] and Funk *et al.* [47]. From the data showed in this table, it comes out that set II yields in general a lower number of rovibrational levels than set I and that their corresponding energy values are, for the X state, less accurate than the published ones. Unfortunately, no published data could be found for the A state.

TABLE III. Calculated rovibrational energy levels of the MgHe ground $X\ ^1\Sigma^+$ and excited $A\ ^1\Pi$ states in cm^{-1}. The results obtained for both potential sets are compared with those of Refs. [30,47].

	$X\ ^1\Sigma^+$				$A\ ^1\Pi$	
(v,J)	Set I	Set II	Ref. [30]	Ref. [47]	Set I	Set II
(0,0)	−0.795	−0.619	−0.769	−0.734		
(0,1)	−0.557	−0.408	−0.531	−0.503	−23.958	−10.259
(0,2)	−0.111	−0.019	−0.088	−0.074	−22.763	−9.379
(0,3)					−20.981	−8.074
(0,4)					−18.624	−6.365
(0,5)					−15.711	−4.283
(0,6)					−12.267	−1.875
(0,7)					−8.324	+0.781
(0,8)					−3.926	+3.518
(0,9)					+0.864	
(1,1)					−4.530	−1.152
(1,2)					−3.751	−0.682
(1,3)					−2.613	+0.038
(1,4)					−1.164	
(1,5)					+0.494	

B. Radiative lifetimes

Among the most commonly accepted and powerful tools for the assessment of the adopted interatomic potentials, transition dipole moments, and dispersion coefficients, and of the computed energy levels and wave functions is perhaps the determination of the level radiative lifetimes.

The purpose here is to determine the radiative lifetime of the $A\ ^1\Pi$ state of MgHe. It is well known from molecular spectra theory that the lifetime $\tau = 1/A(v',J,\Lambda')$ depends on the total spontaneous emission rate [48]

$$A(v',J,\Lambda') = \frac{64\pi^4}{3hc^3}\,\frac{2-\delta_{0,\Lambda'+\Lambda''}}{2-\delta_{0,\Lambda'}} \times \int_0^\infty \nu^3 |\langle \Phi_{v',J,\Lambda'}|D(R)|\Phi_{\epsilon'',J,\Lambda''}\rangle|^2 d\epsilon'' \quad (11)$$

for the transition from the upper bound level (v',J,Λ') of the excited state $A\ ^1\Pi$ to the lower continuum state (ϵ'',J,Λ'') of the ground state $X\ ^1\Sigma^+$. In Eq. (11), δ is the Kronecker symbol.

The lifetime of the closest rotationless vibrational level to the dissociation limit of the MgHe $A\ ^1\Pi$ molecular state should theoretically coincide with the lifetime of the excited $3s3p\ ^1P_1$ state of the isolated Mg atom. Consequently, using the theory described above, our theoretical calculations generated the lifetimes $\tau = 2.096$ ns with set I potentials and $\tau = 2.089$ ns with set II potentials. Both data agree very well with the value $\tau = 2.037$ ns recommended by NIST [49] and with the experimental measurements 2.05 ± 0.05 ns of Reho *et al.* [42], 1.99 ± 0.08 ns of Lurio [50], or 2.2 ± 0.2 ns of Andersen *et al.* [51]. However, some newer calculations predicted 2.14 ns [52,53]. As mentioned by Morton [54], there are at least ten lifetime measurements for the $\lambda_0 = 285.2$ nm upper $3s3p\ ^1P_1$ state, which range, according to this author, from 1.9 to 2.2 ns and have a weighted mean of 2.00 ± 0.03 ns. For a few number of rovibrational levels, our computed $A\ ^1\Pi$ lifetime values are gathered in Table IV.

C. Collision integrals and diffusion coefficients

We have in addition selected for the evaluation of the accuracy of the proposed potential curves to deal with the thermophysical properties of the MgHe gas mixture. More particularly, we suggest scrutinizing the diffusion phenomenon of the ground and excited magnesium atoms in a helium buffer gas and examining the variation law of the diffusion coefficients with temperature. The diffusion of ground and excited atoms is an important physical mechanism observed,

TABLE IV. Lifetimes (in ns) of some rovibrational levels of the MgHe $A\ ^1\Pi$ molecular state. The first and second entries correspond to the set I and set II potentials, respectively.

(v,J)	$J=1$	$J=3$	$J=5$	$J=7$
$v=0$	2.109	2.147	2.106	2.104
	2.094	2.121	2.092	2.091
$v=1$	2.096	2.094	2.091	
	2.089	2.088		

TABLE V. Collision integrals $\overline{\Omega}_{1,1}$, in Å^2, at some specific temperatures. The values related to the $X\ ^1\Sigma^+$ state are compared with data from Ref. [63].

Temperature	$X\ ^1\Sigma^+$			$A\ ^1\Pi$		$B\ ^1\Sigma^+$	
T (K)	Set I	Set II	Ref. [63]	Set I	Set II	Set I	Set II
50	15.44	16.62	15.20	16.60	14.80	32.59	35.43
200	11.61	12.34	11.45	8.52	8.97	22.82	25.20
1000	7.68	8.10	7.51	4.85	4.91	12.73	14.56
3000	5.47	5.55	5.05	3.01	3.03	7.24	8.15
6000	4.30	4.08	3.67	2.11	2.37	4.37	4.96
10 000	3.47	3.11	2.83	1.57	2.03	2.76	3.34

for instance, in the *light-induced drift* phenomenon [55–60], originally described by Gel'mukhanov and Shalagin [61].

According to the Chapman-Enskog approximation for dilute gases, and assuming that Mg is interacting with He along one specific potential curve, the temperature-dependent diffusion coefficient $D(T)$ is expressed in terms of the diffusion integrals $\Omega_{1,1}(T)$ like [62]

$$D(T) = \frac{3}{8n}\sqrt{\frac{\pi k_B T}{2\mu}}\frac{1}{\Omega_{1,1}(T)}, \tag{12}$$

where n is the number density of the helium gas and $\Omega_{1,1}(T)$ is defined as

$$\Omega_{1,1}(T) = \frac{1}{2(k_B T)^3}\int_0^\infty E^2\sigma_D(E)\exp(-E/k_B T)\,dE, \tag{13}$$

with $\sigma_D(E)$ being the quantum-mechanical cross section effective in diffusion

$$\sigma_D = \frac{4\pi}{k^2}\sum_{l=0}^{\infty}(l+1)\sin^2(\eta_{l+1}-\eta_l). \tag{14}$$

Since the Mg atoms interact, while they are excited to the $3s3p$ state, with helium via the $A\ ^1\Pi$ or $B\ ^1\Sigma^+$ potential curves, the total diffusion cross section must have then the statistically weighted value [62]

$$\sigma_D(E) = \tfrac{2}{3}\sigma_D(A) + \tfrac{1}{3}\sigma_D(B). \tag{15}$$

We present in Table V our results of the modified collision integrals $\overline{\Omega}_{1,1} = \Omega_{1,1}/\pi$ for some temperatures, and the X data are compared with those of Partridge, Stallcop, and Levin [63]. The agreement between both results is quite satisfactory, especially at lower temperatures when the set I potential is used. Some values of the diffusion coefficient, calculated at pressure $p = nk_BT = 1$ torr with Eq. (12), are listed in Table VI for a few temperatures lying in the interval 300–1200 K. This table compares our results for the ground state with the measurements of Redko *et al.* [64] and Aref'ev *et al.* [65]. It arises that our data are in excellent agreement with the published experimental values and the relative differences do not exceed 9% with those calculated with set I and 4% with set II. Moreover, the variation law of D with T can easily be determined by fitting our generated MgHe diffusion data with the analytical expression $D(T) \sim \alpha T^\beta$, with α and β being two constant parameters listed in Table VII. Finally, one should note that the absence in literature of the diffusion data of excited Mg atoms in helium deprived us from supporting our generated results.

TABLE VI. Difffusion coefficients at 1-torr pressure in units of 10^2 cm^2 s^{-1}. The measurements are from Refs. [64,65].

Temperature	$Mg(3s^2)+He$			$Mg(3s3p)+He$	
T (K)	Set I	Set II	Measurements	Set I	Set II
300	3.74	3.53	3.40 ± 0.27[a]	3.405	3.120
900	26.0	24.6	24.0[b]	26.37	24.21
1000	31.4	29.8	28.9[b]	32.24	29.65
1200	43.6	41.4	39.6[b]	45.74	42.24

[a]Ref. [64].
[b]Ref. [65].

V. RESULTS AND DISCUSSION

From all the results presented in the previous section, one may conclude that the chosen MgHe potentials as well as the transition dipole moments are fully reliable and, therefore, can be used for any further calculations. It is then the time to solve numerically the radial wave equations (5) and (8), by using the Numerov algorithm [66], to determine the elastic phase shifts $\eta_l(E)$ and the free normalized wave functions $\Phi_{\epsilon,J}(R)$.

A. Width and shift

As already stated before, we utilized the impact approximation method to treat the width w and shift d of the $Mg(3s3p\ ^1P_1 \rightarrow 3s^2\ ^1S_0)$ spectral line when the magnesium atoms are perturbed by helium. After obtaining the elastic phase shifts for each involved molecular symmetry, we have calculated the linewidth and line-shift cross sections, σ_w and σ_d, for energies E ranging from 10^{-6} to 10^{-1} a.u. The total cross sections effective in width and shift are the statistically weighted sums [62]

$$\sigma^{\rm tot}_{w,d}(E) = \tfrac{1}{3}\sigma^{\Sigma\Sigma}_{w,d} + \tfrac{2}{3}\sigma^{\Sigma\Pi}_{w,d}. \tag{16}$$

Hence, the thermally averaged quantities $\langle v\sigma_{w,d}\rangle_{\rm av}$ shown in Eqs. (1) and (2) are given by

$$\langle v\sigma_{w,d}\rangle_{\rm av} = \sqrt{\frac{8}{\mu\pi}}\frac{1}{(k_BT)^{3/2}} \times \int_0^\infty \sigma^{\rm tot}_{w,d}(E)\exp(-E/k_BT)E\,dE. \tag{17}$$

The computed total width and shift cross sections are shown in Fig. 3, from which one can notice the net difference,

TABLE VII. Fitting parameters, α and β (both in S.I. units), for the temperature-dependant diffusion coefficients. The first entry corresponds to set I, the second to set II.

System	$10^8\alpha$	β
$Mg(3s^2)+He$	148.8 ± 2.3	1.775 ± 0.002
	134.6 ± 2.5	1.781 ± 0.003
$Mg(3s3p)+He$	73.5 ± 1.6	1.880 ± 0.003
	63.7 ± 2.0	1.889 ± 0.005

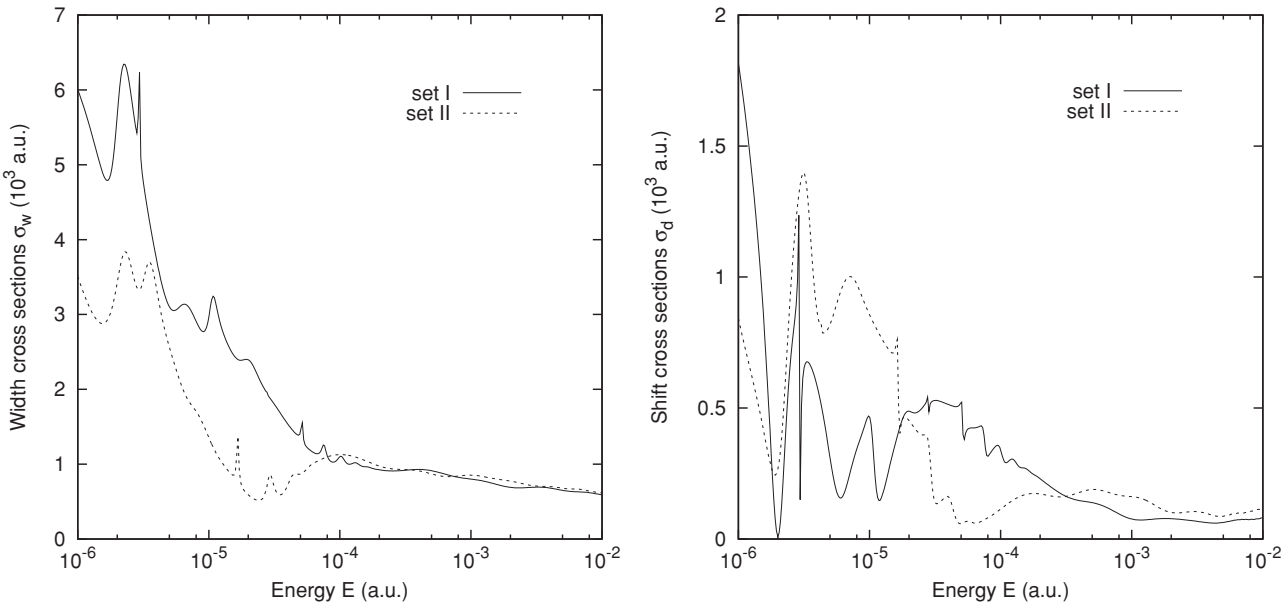

FIG. 3. Variation with energy of the linewidth and line-shift cross sections. Both parameters are calculated with the use of the first and second potential sets.

at smaller energies, between the cross sections calculated from the potentials based on sets I and II. It is particularly noticeable that the so-called resonance peaks do not occur exactly at the same energies. For higher energies, though the curves are smoother, they seem to have the same behavior. Figure 4 illustrates the variation with temperature of the spectral parameters, namely, the linewidth and line-shift rate coefficients, w/n and d/n. It is worth mentioning that set II leads to higher values of the spectral parameters w and d than set I and that the discrepancy between the calculated rates becomes more and more important with increasing temperatures. The relative differences between the rates based on both potential sets could reach 30%. Table VIII lists some values of the width and shift rates at some temperatures where our results are compared with the theoretical data of Bottcher *et al.* [67]. It is finally important to point out that in the temperature range $100 \leqslant T \leqslant 1500$ K, the width-to-shift ratio is found to be nearly 8 to 9.

B. Absorption coefficient

Now, far from the line core, the reduced free-free photoabsorption coefficient $k_r(\nu)$, described through Eq. (7), characterizes the collisional broadening of the spectral line

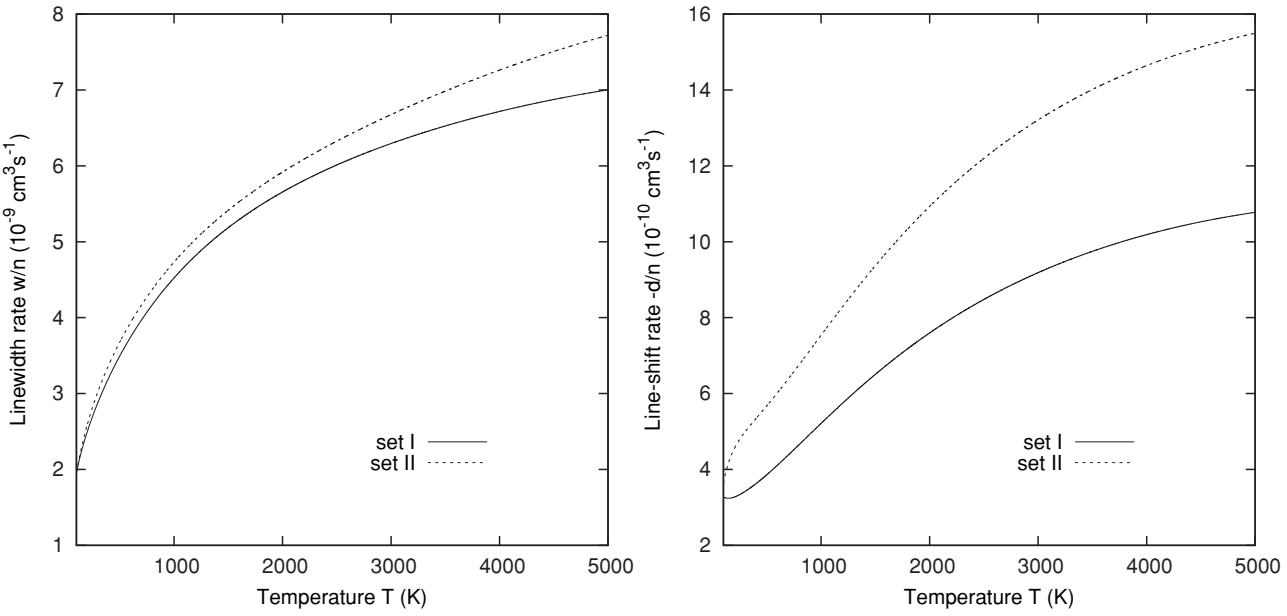

FIG. 4. Linewidth and line-shift rates as a function of temperature calculated from the set I and II potentials.

TABLE VIII. Comparison of our results of linewidth and line-shift rates, for some temperatures, with those of Ref. [67]. All the data are given in units of 10^{-9} cm^3 s^{-1}.

Temperature	w/n			$-d/n$	
T (K)	Set I	Set II	Ref. [67]	Set I	Set II
100	1.956	1.958		0.327	0.364
500	3.496	3.679	3.628	0.386	0.568
1000	4.524	4.733	4.826	0.522	0.754
1500	5.186	5.415	4.884	0.651	0.937

shape in the wings. For the MgHe case, the probability ϖ this diatomic system possesses to form a molecule is given by [12]

$$\varpi = \xi \frac{2S_{\mathrm{MgHe}} + 1}{(2S_{\mathrm{Mg}} + 1)(2S_{\mathrm{He}} + 1)}, \tag{18}$$

where $\xi = 1$ for the $B\,^1\Sigma^+$ state and $\xi = 2$ for $A\,^1\Pi$ state, and $S_{\mathrm{MgHe}} = 1$, $S_{\mathrm{Mg}} = 1$, and $S_{\mathrm{He}} = 1$ are the spin multiplicities for the MgHe molecule and Mg and He atoms. The numerical resolution of the radial wave equation (8) leads to the upper and lower free energies, ϵ' and ϵ'', and to the corresponding wave functions $\Phi_{\epsilon,J}(R)$, which allow the computation of the matrix elements $\langle \Phi_{\epsilon',J} | D(R) | \Phi_{\epsilon'',J} \rangle$. We used in these calculations a maximum rotational number $J_{\max} = 250$ and a frequency step $\Delta\nu = 10\,\mathrm{cm}^{-1}$.

Figure 5 illustrates, for wavelengths laying between 260 and 310 nm, the MgHe photoabsorption profiles at three distinct temperatures: 1000, 2000, and 3000 K. The upper curves are those obtained with set I potentials and the lower curves with set II potentials. Both plots present similar shapes, which consist of two wings around the unperturbed Mg($3s3p \leftarrow 3s^2$) wavelength, $\lambda_0 = 285.2$ nm. The calculations revealed that the blue wing arises from the $B\,^1\Sigma^+ \leftarrow X\,^1\Sigma^+$ transitions and the red wing from the $A\,^1\Pi \leftarrow X\,^1\Sigma^+$ transitions. They also brought to light that the red wings are particularly alike, that is, with a smooth profile of the same magnitude and increasing in intensity with temperature. Whereas, the blue side exhibits at temperatures beyond approximately $T \sim 1800$ K, an apparent satellite structure, mixed with undulations and located around different wavelengths, i.e., $\lambda \simeq 276$ nm when the first data set is used, and $\lambda \simeq 272$ nm when the second data set is used. At this point, one should note that both profiles are remarkably sensitive to the temperature and that the satellite based on set I seems to be more intense than the one based on set II. The above satellite positions have already been predicted classically, namely, 273 and 268 nm, respectively, and the relative differences do not exceed in both cases 2%. Moreover, we display in Fig. 6 the absorption spectra at the same temperature $T = 3000$ K. The full and dotted lines correspond to the set I and II calculations, respectively. It appears that both sets yield in the red wing almost the same profile, but in the opposite wing their sensitivity to the details of the potentials, probably to their repulsive walls, is demonstrated.

In Figure 7, we represent, in arbitrary units, the modified reduced absorption coefficient $k_r(\Delta\omega)(\Delta\omega)^2$, calculated at 800 K, as a function of the frequency detuning $\Delta\omega = \omega_0 - \omega$ (in cm^{-1}) from the Mg atomic resonance line. Since the potential difference could predict the possible occurrence of

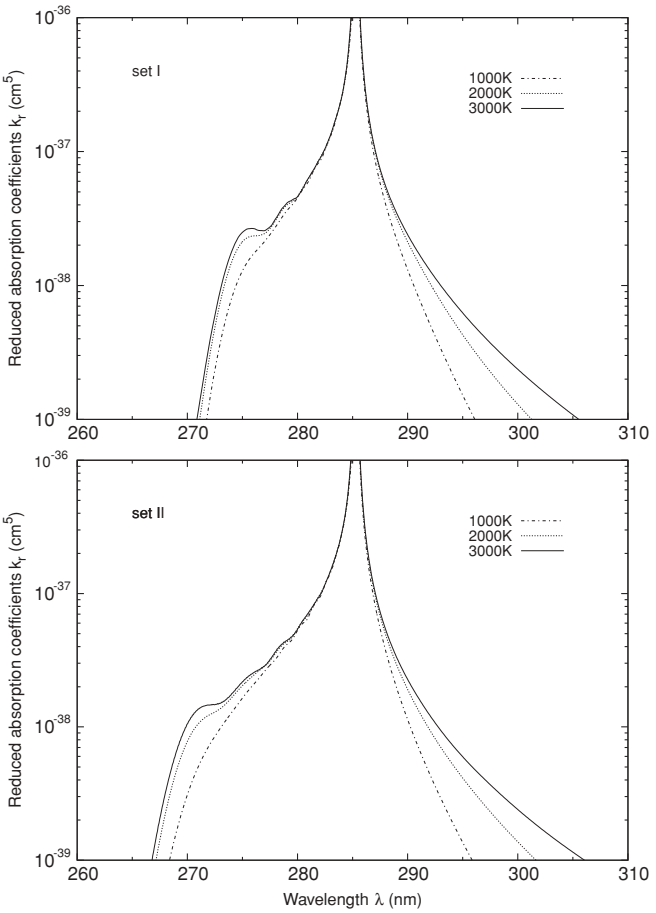

FIG. 5. MgHe reduced photoabsorption coefficients $k_r(\nu)$ at three temperatures: $T = 1000$, 2000, and 3000 K, generated with set I and II potentials.

a satellite close to the wavelength 413 nm, which is outside the initial wavelength domain toward the visible spectrum, it is reasonable to choose this modification, already suggested by Lyyra, Sando, and Kleiber [68], to be able to highlight the weak satellites and to enhance the representation of the

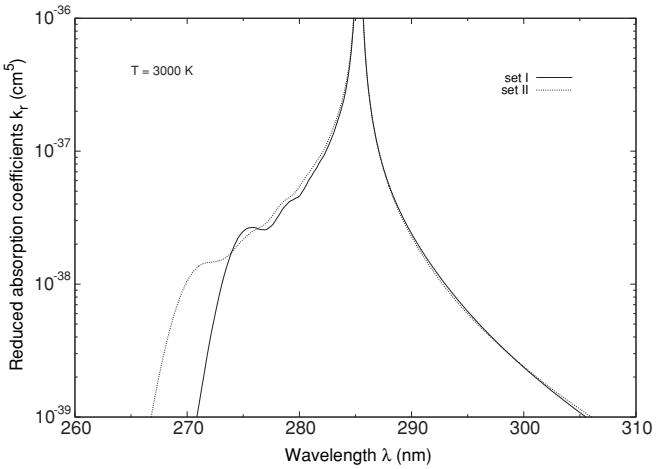

FIG. 6. Comparison of the MgHe photoabsorption profiles at one fixed temperature $T = 3000$ K when the calculations are based on the set I and II potentials.

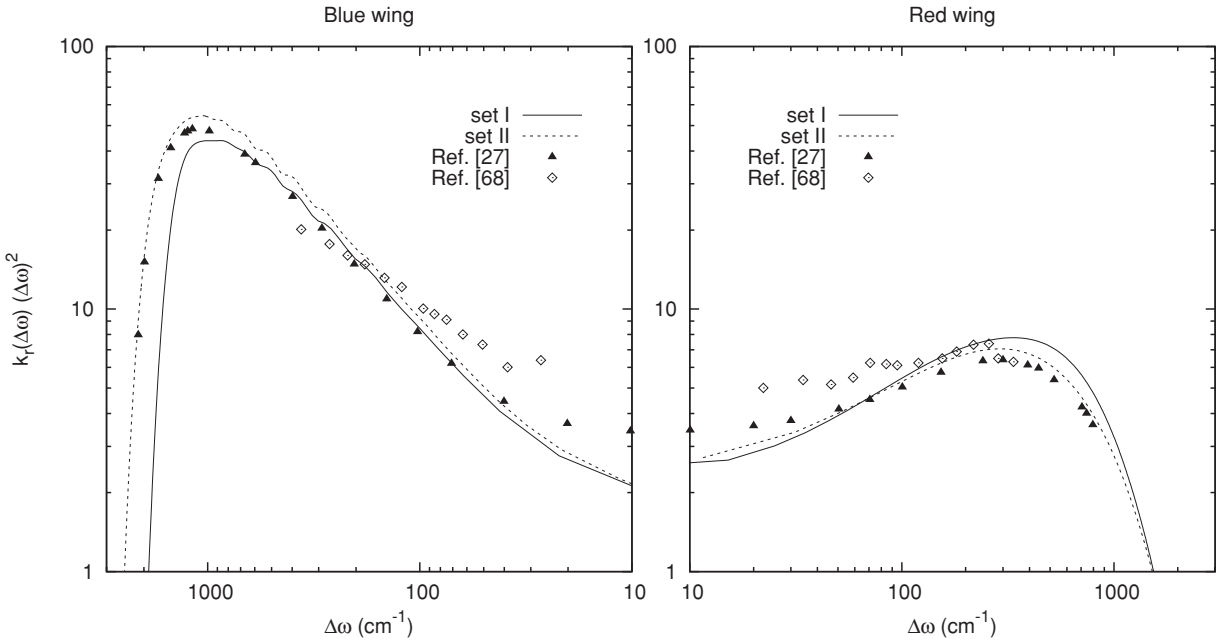

FIG. 7. Modified reduced absorption coefficients $k_r(\Delta\omega)(\Delta\omega)^2$ at $T = 800$ K as a function of detuning $\Delta\omega = |\omega_0 - \omega|$. The profiles are based on the use of the two potential sets. The full and empty symbols represent, respectively, theoretical data [27] and experimental measurements at 700 K [68].

profile. Indeed, there are sometimes broad low extrema in the potential differences which may not be visible in the $k(\nu)$ spectrum, especially if they are situated in the marginally thermally accessible regions [69]. Whether the first or the second interatomic potential set is utilized, our calculations confirmed the occurrence of satellite peaks in both sides of the profile. In the blue-wing spectra, the peaks are found close to the detuning $\Delta\omega \sim 1000\,\text{cm}^{-1}$, while, in the red wing, weaker peaks are located in the vicinity of the value $\Delta\omega \sim 300\,\text{cm}^{-1}$.

Furthermore, by applying at $T = 800$ K fully quantum-mechanical close-coupling calculations, Paul-Kwiek and Czuchaj [27] obtained the theoretical results which are plotted in Fig. 7. We have also represented in the same figure the experimental data measured at $T \sim 700$ K by Lyyra *et al.* [68]. Note that our values of the far blue- and red-wing spectra have been normalized so that they cope with the published data. The concordance of all the results is quite satisfactory.

VI. CONCLUSION

In this work, we tried to analyze the effect of the interatomic potentials on the line-core and far-wing emission and absorption profiles of the $\text{Mg}(3s3p \leftrightarrow 3s^2) - \text{He}(1s^2)$ system. To test the accuracy of our constructed potentials, based on two different sets, we have calculated the excited-level lifetimes, collision integrals, and temperature-dependant diffusion coefficients. The agreement between our results and other published values is noticeable. We have then performed quantum-mechanical calculations of the linewidth and line-shift parameters as well as the absorption coefficient for temperatures ranging from 100 to 3000 K. We could point out that only the free-free transitions are dominant and that the profile presents beyond approximately 1800 K a satellite structure in the blue wing near the wavelengths 272 or 276 nm, depending on the potential set used. Finally, the expected weak satellite in the red wing near 413 nm has been discussed and all the results are compared with previous calculations and measurements.

ACKNOWLEDGMENTS

The authors thank Dr. E. Paul-Kwiek, F. Cargnoni, and K. Lehmann for the data points of the MgHe potentials and TDMs they provided. They are also very grateful to Prof. M. Lyyra and Dr. K. Alioua for helpful discussions and to the referees for their constructive comments and suggestions. One of the authors (M.B.) wishes to acknowledge the valuable advices of Prof. Alex Dalgarno from Harvard-Smithsonian Center for Astrophysics and of Dr. Monique Aubert-Frécon from LASIM to improve this paper.

[1] N. F. Allard and J. F. Kielkopf, Rev. Mod. Phys. **54**, 1103 (1982).
[2] J. Szudy and W. E. Baylis, Phys. Rep. **266**, 127 (1996).
[3] F. Stienkemeier, J. Higgins, C. Callegari, S. I. Kanorsky, W. E. Ernst, and G. Scoles, Z. Phys. D **38**, 253 (1996).
[4] A. Nakayama and K. Yamashita, J. Chem. Phys. **114**, 780 (2001).
[5] A. Hernando, M. Barranco, R. Mayol, M. Pi, and F. Ancilotto, Phys. Rev. B **78**, 184515 (2008).
[6] R. Guardiola, J. Navarro, D. Mateo, and M. Barranco, J. Chem. Phys. **131**, 174110 (2009).
[7] K. B. Whaley, Int. Rev. Phys. Chem. **13**, 41 (1994).

[8] J. P. Toennies and A. F. Vilesov, Annu. Rev. Phys. Chem. **49**, 1 (1998).
[9] M. Barranco, R. Guardiola, S. Hernández, R. Mayol, J. Navarro, and M. Pi, J. Low Temp. Phys. **142**, 1 (2006).
[10] F. O. Ellison, J. Am. Chem. Soc. **85**, 3540 (1963).
[11] H.-K. Chung, K. Kirby, and J. F. Babb, Phys. Rev. A **60**, 2002 (1999).
[12] H.-K. Chung, K. Kirby, and J. F. Babb, Phys. Rev. A **63**, 032516 (2001).
[13] M. Bouledroua, A. Dalgarno, and R. Côté, Phys. Rev. A **65**, 012701 (2001).
[14] P. S. Erdman, C. W. Larson, M. Fajardo, K. M. Sando, and W. C. Stwalley, J. Quant. Spectrosc. Radiat. Transfer **88**, 447 (2004).
[15] C. Vadla, R. Beuc, V. Horvatic, M. Movre, A. Quentmeier, and K. Niemax, Eur. Phys. J. D **37**, 37 (2006).
[16] C. Vadla, V. Horvatic, and K. Niemax, Appl. Phys. B **84**, 523 (2006).
[17] F. Talbi, M. Bouledroua, and K. Alioua, Eur. Phys. J. D **50**, 141 (2008).
[18] N. F. Allard, F. Allard, P. H. Hauschildt, J. F. Kielkopf, and L. Machin, Astron. Astrophys. **411**, L473 (2003).
[19] C. Zhu, J. F. Babb, and A. Dalgarno, Phys. Rev. A **71**, 052710 (2005).
[20] C. Zhu, J. F. Babb, and A. Dalgarno, Phys. Rev. A **73**, 012506 (2006).
[21] K. Alioua and M. Bouledroua, Phys. Rev. A **74**, 032711 (2006).
[22] F. Shindo, J. F. Babb, K. Kirby, and K. Yoshino, J. Phys. B **40**, 2841 (2007).
[23] N. F. Allard, F. Spiegelman, and J. F. Kielkopf, Astron. Astrophys. **465**, 1085 (2007).
[24] D. F. T. Mullamphy, G. Peach, V. Venturi, I. B. Whittingham, and S. J. Gibson, J. Phys. B **40**, 1141 (2007).
[25] K. Alioua, M. Bouledroua, A. R. Allouche, and M. Aubert-Frécon, J. Phys. B **41**, 175102 (2008).
[26] E. Czuchaj, F. Rebentrost, H. Stoll, and H. Preuss, Theor. Chem. Acc. **100**, 117 (1998).
[27] E. Paul-Kwiek and E. Czuchaj, Eur. Phys. J. D **3**, 163 (1998).
[28] B. Kerkeni, P. S. Barklem, A. Spielfiedel, and N. Feautrier, J. Phys. B **37**, 677 (2004).
[29] J. C. Holtgrave and P. J. Wolf, Phys. Rev. A **72**, 012711 (2005).
[30] C. C. Lovallo and M. Klobukowski, Chem. Phys. Lett. **373**, 439 (2003).
[31] M. Baranger, Phys. Rev. **111**, 481 (1958).
[32] M. Baranger, Phys. Rev. **111**, 494 (1958); **112**, 855 (1958).
[33] P. S. Julienne and F. H. Mies, Phys. Rev. A **34**, 3792 (1986).
[34] T. Orlikowski, Eur. Phys. J. D **28**, 187 (2004).
[35] K. M. Sando and A. Dalgarno, Mol. Phys. **20**, 103 (1971).
[36] M. Borkowski, R. Ciuryło, P. S. Julienne, S. Tojo, K. Enomoto, and Y. Takahashi, Phys. Rev. A **80**, 012715 (2009).
[37] T. Grycuk, W. Behmenburg, and V. Staemmler, J. Phys. B **34**, 245 (2001).
[38] W. Behmenburg, A. Kaiser, H. Bettermann, T. Grycuk, and V. Staemmler, J. Phys. B **35**, 747 (2002).
[39] G. Herzberg, *Molecular Spectra and Molecular Structure*, Vol. I: *Spectra of Diatomic Molecules*, (van Nostrand, Princeton, 1963).
[40] R. J. Hinde, J. Phys. B **36**, 3119 (2003).
[41] M. Mella, G. Calderoni, and F. Cargnoni, J. Chem. Phys. **123**, 054328 (2005).
[42] J. Reho, U. Merker, M. R. Radcliff, K. K. Lehmann, and G. Scoles, J. Chem. Phys. **112**, 8409 (2000).
[43] H. Pauly, in *Atom-Molecule Collision Theory*, edited by R. B. Bernstein (Plenum, New York, 1979).
[44] J. Mitroy and J. Y. Zhang, Mol. Phys. **106**, 127 (2008).
[45] R. J. Le Roy, LEVEL 7.4 program, University of Waterloo, Chemical Physics Research Report, 2001 (unpublished).
[46] G. F. Gribakin and V. V. Flambaum, Phys. Rev. A **48**, 546 (1993).
[47] D. J. Funk, W. H. Breckenridge, J. Simons, and G. Chałasi ński, J. Chem. Phys. **91**, 1114 (1989).
[48] B. H. Bransden and C. J. Joachain, *Physics of Atoms and Molecules* (Longman, London, 1983).
[49] Yu. Ralchenko, A. E. Kramida, and J. Reader (NIST ASD Team), NIST Atomic Spectra Database, v. 3.1.5, 2008.
[50] A. Lurio, Phys. Rev. **136**, A376 (1964).
[51] T. Andersen, J. Desesquelles, K. A. Jessen, and G. Sørensen, J. Quant. Spectrosc. Radiat. Transfer **10**, 1143 (1970).
[52] P. Jönsson and C. Froese Fischer, J. Phys. B **30**, 5861 (1997).
[53] P. Jönsson, C. Froese Fischer, and M. R. Godefroid, J. Phys. B **32**, 1233 (1999).
[54] D. C. Morton, Astrophys. J. Suppl. Ser. **149**, 205 (2003).
[55] T. P. Redko, Opt. Spectrosc. **52**, 461 (1982).
[56] W. A. Hamel, J. E. M. Haverkort, H. G. C. Werij, and J. P. Woerdman, J. Phys. B **19**, 4127 (1986).
[57] T. P. Redko, Opt. Spectrosc. **61**, 592 (1986).
[58] S. N. Atutov and A. M. Shalagin, Sov. Astron. Lett. **14**, 284 (1988).
[59] A. I. Parkhomenko, Opt. Spectrosc. **67**, 14 (1989).
[60] S. N. Atutov, B. V. Bondarev, S. M. Kobtzev, P. V. Kolinko, S. P. Podjachev, and A. M. Shalagin, Opt. Commun. **115**, 276 (1995).
[61] F. Kh. Gel'mukhanov and A. M. Shalagin, JETP Lett. **29**, 711 (1979).
[62] E. A. Mason and E. W. McDaniel, *Transport Properties of Ions in Gases* (Wiley, New York, 1988).
[63] H. Partridge, J. R. Stallcop, and E. Levin, J. Chem. Phys. **115**, 6471 (2001).
[64] T. P. Redko, I. M. Rusinov, and A. B. Blagoev, J. Phys. B **26**, 107 (1993).
[65] K. M. Aref'ev, M. A. Guseva, and B. M. Khomchenkov, High Temp. **25**, 174 (1987).
[66] B. Numerov, Pub. Observ. Central Astrophys. Russ. **2**, 188 (1933).
[67] C. Bottcher, K. K. Docken, and A. Dalgarno, J. Phys. B **8**, 1756 (1975).
[68] A. M. Lyyra, K. M. Sando, and P. D. Kleiber, Phys. Rev. A **35**, 915 (1987).
[69] A. M. Lyyra (private communication).